Chinese Journal of Catalysis 38 (2017) 1166–1173

available at www.sciencedirect.com

ScienceDirect

journal homepage: www.elsevier.com/locate/chnjc

Article

Ni/Al_2O_3 catalysts derived from spinel $NiAl_2O_4$ for low-temperature hydrogenation of maleic anhydride to succinic anhydride

Jie Li, Yuanhang Ren, Bin Yue #, Heyong He *

Department of Chemistry and Shanghai Key Laboratory of Molecular Catalysis and Innovative Materials, Collaborative Innovation Center of Chemistry for Energy Materials, Fudan University, Shanghai 200433, China

ARTICLE INFO

Article history:
Received 22 February 2017
Accepted 19 April 2017
Published 5 July 2017

Keywords:
Maleic anhydride
Succinic anhydride
Hydrogenation
Nickel
Spinel

ABSTRACT

Ni/Al_2O_3 catalysts were derived from spinel $NiAl_2O_4$ with different Ni content ((2.5, 5 and 7.5) wt%). The catalysts were obtained by H_2 reduction and were investigated for the low-temperature hydrogenation of maleic anhydride (MA) to produce succinic anhydride (SA). The characterization results showed that Ni^0 active sites were mainly derived during the H_2 reduction from spinel $NiAl_2O_4$. Among the catalysts studied, employing the optimum preparation and reaction conditions with $Ni(5\%)/Al_2O_3$ yielded the highest catalytic performance. A near-100% conversion of MA and ~90% selectivity to SA were achieved at 120 °C and 0.5 MPa of H_2 with a weighted hourly space velocity (MA) of 2 h^{-1}.

1. Introduction

The hydrogenation of maleic anhydride (MA) is an important reaction for the production of valuable intermediates such as succinic anhydride (SA) and γ-butyrolactone (GBL) [1–5]. The hydrogenation of MA to yield such intermediates has been investigated at temperatures of 100–200 °C over a variety of catalysts, which include those based on noble metals, such as Pd/Al_2O_3 [6], Ru complexes [7], Ru/C [8], and Au/TiO_2 [9]. Noble metal-based catalysts are highly active for the MA hydrogenation but relatively expensive. Cheaper Cu- and Ni-based catalysts have, therefore, attracted much attention [10,11]. Various supported Cu catalysts, such as Cu/SiO_2 [1], Cu/ZrO_2 [3] and Cu-Ce-Al_2O_3 [12], favored the formation of GBL during longer reactions under higher temperatures (200–260 °C). Compared with the Cu-based catalysts, those that were Ni-based showed a higher catalytic efficiency in the low-temperature hydrogenation of MA [13]. Ni-based catalysts, such as Ni/CeO_2 [4], Ni/SiO_2 [13], Ni/H-BEA [14], Ni/TiO_2 [15], Ni/Al_2O_3 [16], and Ni/SiO_2-Al_2O_3 [17], have generally been investigated at temperatures of 170–220 °C. The main disadvantages of the supported Ni catalysts include high Ni-loading, and deactivation of the catalyst at high reaction temperatures [10,13–20]. Moreover, Bertone *et al.* [21] investigated the Cu-modified Ni/SiO_2-Al_2O_3 catalysts and found that the Ni^0 active species exhibited high catalytic activity, but they observed deactivation during 3 h of testing. Therefore, it is highly desirable to develop novel Ni-based catalytic systems with enhanced activity and stability for the hydrogenation of MA at low temperatures.

It is well known that spinel-type oxides such as $NiAl_2O_4$ may be employed as a catalyst precursor for various catalytic reactions. Spinel-derived Ni/Al_2O_3 catalysts exhibited good catalytic activity and stability during methane reforming and the hy-

* Corresponding author. Tel: +86-21-65643916; Fax: +86-21-55665572; E-mail: heyonghe@fudan.edu.cn
# Corresponding author. Tel: +86-21-65642779; Fax: +86-21-65338041; E-mail: yuebin@fudan.edu.cn
This work was supported by the National Natural Science Foundation of China (21173050, 21371035) and SINOPEC (X514005).
DOI: 10.1016/S1872-2067(17)62844-4 | http://www.sciencedirect.com/science/journal/18722067 | Chin. J. Catal., Vol. 38, No. 7, July 2017

drogenation of benzene because the metallic Ni species were well dispersed [22]. However, little work focusing on catalysts derived from spinel Ni composites in the hydrogenation of MA has been reported.

Herein, therefore, we report on a series of spinel-derived catalysts prepared with varying Ni content. The effects of Ni content and dispersion, particle size and reduction degree on the catalytic activity in the hydrogenation of MA are investigated. Under optimized preparation and reaction conditions, Ni(5%)/Al_2O_3 exhibited the highest activity during the low-temperature hydrogenation of MA.

2. Experimental

2.1. Catalyst preparation

Pseudoboehmite (Shangdong City Star Petroleum Chemical Technology Co. Ltd., China) was calcined at 750 °C for 3 h and used as the Al_2O_3 support. Ni/Al_2O_3 catalysts with (2.5, 5.0 and 7.5) wt% Ni were prepared by the wet impregnation method. A typical procedure involved 2.8 mL (2.5% Ni), 5.6 mL (5.0% Ni) or 8.4 mL (7.5% Ni) of 0.32 mol/L aqueous solution of $Ni(NO_3)_2{\cdot}6H_2O$ being added to a suspension containing 2 g of Al_2O_3 and 32 mL of H_2O. The mixture was then stirred for 12 h at room temperature. After impregnation, water in the mixture was removed using a rotary evaporator operating at 70 °C. The samples were dried at 120 °C for 12 h and then calcined at 750 °C for 3 h.

2.2. Characterization of the catalysts

Elemental analysis was performed by a Thermo Elemental IRIS Intrepid inductively coupled plasma atomic emission spectrometer (ICP-AES). N_2 physisorption experiments were carried out with a Quantachrome Quadrasorb S1 apparatus. Powder X-ray diffraction (XRD) patterns were obtained on a Bruker D8 Advance X-ray diffractometer using Cu $K_{\alpha 1}$ radiation (λ = 0.15406 nm) operated at 40 eV and 40 mA. X-ray photoelectron spectroscopic (XPS) experiments were carried out using a Perkin-Elmer PHI 5000C ESCA system. H_2 temperature-programmed reduction (H_2-TPR) and CO temperature-programmed desorption (CO-TPD) were performed using a Micromeritics Chemisorb 2720. UV-Vis DRS spectra were obtained from a JASCO UV550 UV-Vis absorption spectrometer. The FT-IR spectra were recorded by a Nicolet Nexus 470 infrared instrument using KBr discs. ^{27}Al MAS NMR spectra were acquired using a Bruker Advance DSX400 spectrometer.

2.3. Catalytic activity

The MA hydrogenation was performed in a fixed-bed reactor. In a typical experiment, catalysts (0.25 g, 60–80 mesh) were loaded into the center of the reactor tube between two silica sand layers and activated *in situ* by a flow of 5% H_2–95% Ar (50 mL/min) at the desired reduction temperature (650–750 °C) for 2 h. After reduction, the reactor was cooled to the selected reaction temperature (100–160 °C) and the feed (15 wt% MA dissolved in GBL) was continuously introduced into the reactor by a syringe pump. Varying the mass of catalyst while holding the feed flow rate constant provided different values of weighted hourly space velocity (WHSV), for which reactions were carried out at 120 °C. Products were collected at intervals of 1 h and analyzed by gas chromatography (GC) using a HP-5 capillary column and a flame ionization detector. The conversion of MA and the selectivity to SA and GBL were calculated as follows:

$$\text{Conversion (\%)} = (MA_{in} - MA_{out})/MA_{in} \times 100 \quad (1)$$

$$\text{Selectivity (i) (\%)} = Product_{i,out}/(MA_{in} - MA_{out}) \times 100 \quad (2)$$

where MA_{in}, MA_{out} and $Product_{i,out}$ represent the molar concentration of the reactant at the inlet and the outlet, and that of the products at the outlet, respectively.

3. Results and discussion

3.1. Catalyst characterization

Textural properties of the calcined catalysts and the Al_2O_3 support are listed in Table 1. The total Ni-loading determined by ICP-AES was consistent with the calculated values. The surface area and pore volume of the Al_2O_3 support were 214 m^2/g and 1.14 cm^3/g, respectively. For the calcined catalysts, the surface area and pore volume decreased with increasing Ni content, which may have been caused by the incorporated Ni species [23].

The XRD patterns of the Al_2O_3 support and the calcined catalysts are shown in Fig. 1. The diffraction peaks at 2θ = 37.4°, 39.7°, 45.8° and 67.3° may be attributed to (311), (222), (400) and (522) diffractions of γ-Al_2O_3 (PDF No. 04-0880), respectively [5,24–26]. Compared with the diffraction pattern of Al_2O_3, three new peaks at 2θ = 19.1°, 31.6° and 60.2° were observed in the calcined catalysts and attributed to (111), (220) and (511) diffractions of spinel $NiAl_2O_4$ (PDF No. 10-0339), respectively, suggesting the formation of spinel $NiAl_2O_4$. Moreover, the peak at $2\theta \approx 60°$ slightly shifted to a higher value (60.2°) for all the calcined catalysts, indicating the formation of the defect $NiAl_2O_4$ phase [27,28]. The diffraction peaks at 37°–39° may be attributed to NiO and/or $NiAl_2O_4$ phases which could not be definitely distinguished [27]. $NiAl_2O_4$ also exhibited diffraction peaks at $2\theta \approx 66°$ though careful analysis suggested that these differed from peaks in this vicinity exhibited by the Al_2O_3 support. Increasing the Ni-loading from 2.5% to 7.5% slightly decreased the diffraction peaks, perhaps because of the formation of $NiAl_2O_4$ and because the ionic radius of Ni is greater than that of Al [28].

Table 1
Physicochemical properties of the Al_2O_3 support and the calcined Ni/Al_2O_3 catalysts.

Sample	Metal loading[a] (%)	S_{BET} (m^2/g)	V_{Pore} (cm^3/g)
Al_2O_3	—	214	1.14
Ni(2.5%)/Al_2O_3	2.5	180	1.02
Ni(5%)/Al_2O_3	4.9	157	0.89
Ni(7.5%)/Al_2O_3	7.2	129	0.82

[a] Analyzed by ICP-AES.

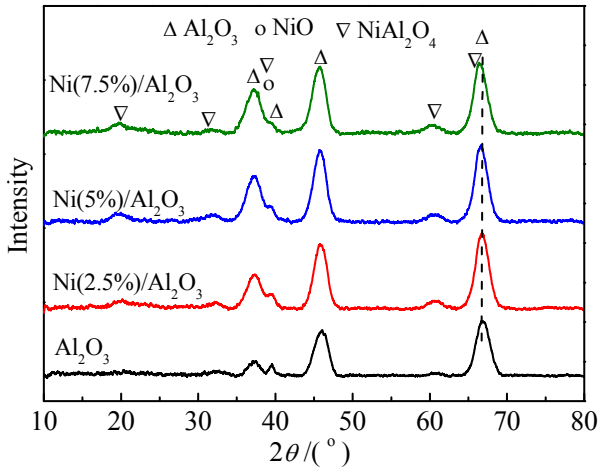

Fig. 1. XRD patterns of the Al_2O_3 support and the calcined catalysts.

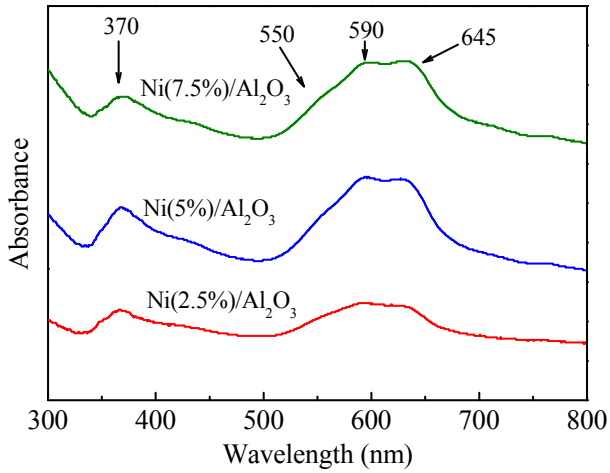

Fig. 3. UV-Vis DRS results for the calcined catalysts.

The XPS results for the calcined catalysts are shown in Fig. 2. The observed peaks can be interpreted as a combination of two Ni $2p_{3/2}$ peaks with binding energies of ~854.9 and ~858.2 eV, which can be assigned to the Ni^{2+} in NiO and Ni^{2+} in $NiAl_2O_4$, respectively [29,30]. The closer proximity of the observed peaks to 858.2 eV indicated that the main phase was spinel $NiAl_2O_4$.

The near-identical UV-Vis DRS results for the calcined catalysts are shown in Fig. 3. The band at 370 nm can be attributed to the octahedral coordinated Ni^{2+} species in the NiO lattice, while the bands at 590–645 nm and a shoulder at 550 nm are associated with the tetrahedral coordinated Ni^{2+} species in the $NiAl_2O_4$ lattice [31,32]. Moreover, based on the relative intensity of the absorption bands at 550–645 nm and 370 nm, the tetrahedral Ni^{2+} ion content was found to be higher than that of octahedral Ni^{2+} ions.

The FT-IR spectra of the calcined catalysts are shown in Fig. 4. The spinel's presence in the catalysts was indicated by the appearance of two bands typical of $NiAl_2O_4$ spinel at 520 and 730 cm^{-1} [33], which are attributed to M–O (Ni–O, Al–O) stretching vibrations in octahedral and tetrahedral environments, respectively [34].

These characterization results suggest that the calcined Ni(2.5%)/Al_2O_3, Ni(5%)/Al_2O_3 and Ni(7.5%)/Al_2O_3 catalysts mainly comprised of a $NiAl_2O_4$ phase with a minor NiO phase.

The results of the H_2-TPR analysis are shown in Fig. 5, where the three catalysts displayed a reduction shoulder at 500–550 °C and a main reduction peak at 750 °C. However, the shoulder was much more pronounced for the Ni(7.5%)/Al_2O_3 (Fig. 5(c)) catalyst. Generally, the reduction peak at 750 °C is assigned to the reduction of $NiAl_2O_4$, while the peak at 500–550 °C is ascribed to the reduction of NiO, which has a strong interaction with the Al_2O_3 support [22,31,35]. For all the calcined catalysts, the H_2-TPR curve returned to the baseline level after treatment at 750 °C for 2 h and no peak was observed above 750 °C. This indicated that the Ni species were fully reduced following 2 h at 750 °C, in agreement with that reported by Numaguchi *et al.* [36].

The CO-TPD results obtained for the catalysts following 2 h of H_2 reduction at 750 °C are shown in Fig. 6. Desorption peaks near to 105 °C (weakly chemisorbed CO) and 360 °C (moderately chemisorbed CO) were observed for all of the catalysts [37]. The area under the CO-TPD desorption peaks can be correlated with the amounts of metallic Ni species [37], and the amount of desorbed CO was found to increase with increasing Ni content. Ni-dispersion was calculated using the CO-TPD desorption peaks by assuming an equal surface stoichiometry of CO:Ni (Table 2) [5]. The calculated Ni-dispersion decreased

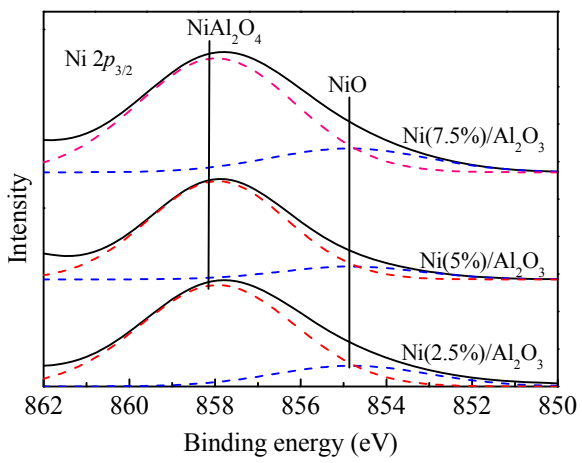

Fig. 2. XPS spectra for the calcined catalysts in the Ni 2*p* region.

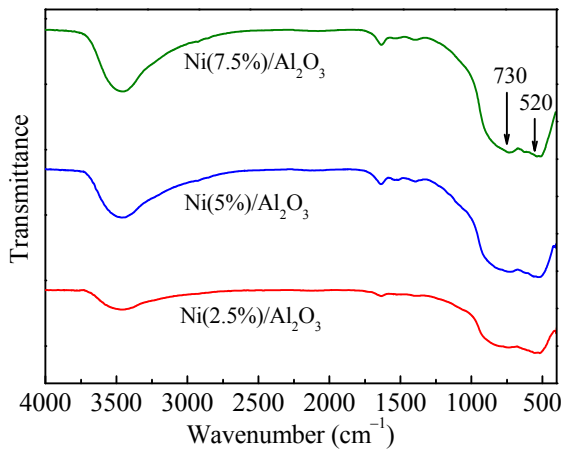

Fig. 4. FT-IR spectra of the calcined catalysts.

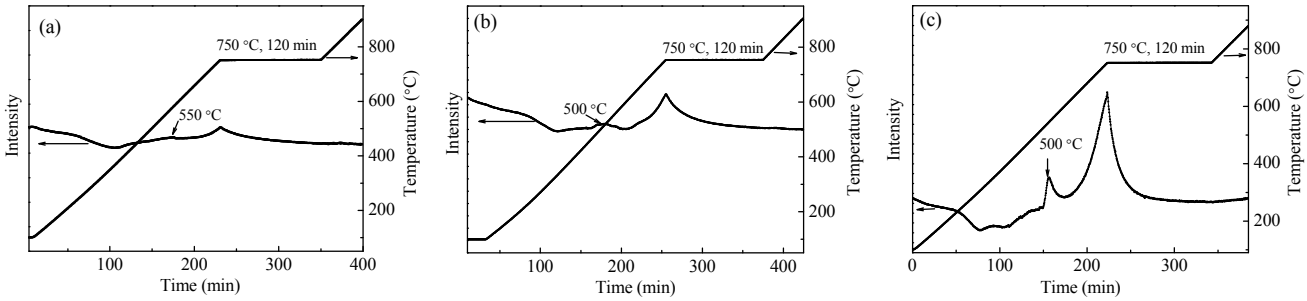

Fig. 5. H_2-TPR results for calcined Ni(2.5%)/Al_2O_3 (a); Ni(5%)/Al_2O_3 (b) and Ni(7.5%)/Al_2O_3 (c) catalysts.

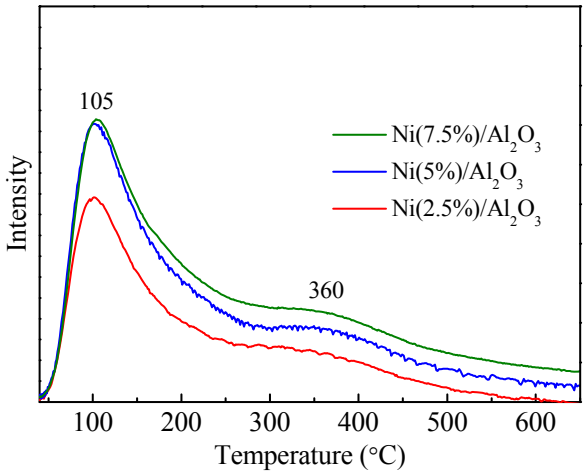

Fig. 6. CO-TPD for the three Ni/Al_2O_3 catalysts after being reduced at 750 °C for 2 h.

with increasing Ni content, indicating that Ni species congregated at higher Ni-loadings. The CO chemisorption analysis was also used to produce the Ni particle size estimates of 8.0, 12.8 and 15.7 nm for the (2.5, 5.0 and 7.5)% Ni content, respectively. These findings were consistent with the XRD results (Table 2).

The XRD patterns of the reduced catalysts in Fig. 7 show the metallic Ni and the Al_2O_3 phases were observed but that no distinct diffractions corresponding to $NiAl_2O_4$ were detected. For the highest Ni content catalyst (7.5%), the diffractions observed at 2θ = 44.5°, 51.8° and 76.4° were attributed to (111), (200) and (220) of metallic Ni phases (PDF No. 04-0850), respectively. The results for the 5% Ni catalyst showed peaks in the same locations, but they were slightly broader and weaker, suggesting that the metallic Ni particle sizes were smaller. No metallic Ni phases were observed for the 2.5% Ni catalyst, which may have been because this sample exhibited the smallest Ni^0 particle size and the lowest amount of metallic Ni species. The average particle sizes (Table 2), calculated from Ni(200) (2θ = 51.8°) diffraction peaks using the Scherrer equation, for the reduced (5.0 and 7.5)% Ni catalysts were ~12.5 and ~15.8 nm, respectively.

Table 2
Ni-dispersion and particle size for the three catalysts after being reduced at 750 °C for 2 h.

Catalyst	Dispersion[a] (%)	D_{Ni}[b] (nm)	D_{Ni}[c] (nm)
Ni(2.5%)/Al_2O_3	12.5	8.0	—
Ni(5%)/Al_2O_3	7.9	12.8	12.5
Ni(7.5%)/Al_2O_3	6.4	15.7	15.8

[a] Dispersion (%) = surface Ni^0 atom/(total Ni^0 atom) × 100.
[b] Determined by CO chemisorption.
[c] Calculated from Ni(200) (2θ = 51.8°) diffraction peaks using the Scherrer equation.

3.2. Catalytic activity

Fig. 8 shows the catalytic performance of the three catalysts under conditions of 120 °C, 0.1 or 0.5 MPa of H_2 and WHSV (MA) = 2 h^{-1}. MA conversion generally increased with increasing H_2 pressure while the 5.0% catalyst showed the highest catalytic activity achieving a near-100% conversion of MA at 0.5 MPa of H_2. The relatively lower activity of the other catalysts was particularly notable during the lower H_2 pressure tests. The increase in catalytic activity between (2.5 and 5.0)% Ni samples may have been caused by an increase of Ni^0 active sites. However, the large particle size of Ni^0 observed for higher loading in the 7.5% Ni sample resulted in a decrease of hydrogenation activity. Therefore, both the amount and the particle size of Ni^0 species impacted catalytic activity [4,17]. It is noteworthy that Ni-loading is generally in the range of (7–10)% for supported Ni catalysts, such as Ni/CeO_2 [4] and Ni/diatomite [20]. Indeed, Guo *et al.* [20] studied the effect of Ni-loading on MA hydrogenation over Ni/diatomite catalysts and found a 7% Ni-loading provided the highest catalytic activity.

The selectivities to SA and GBL shown in Fig. 8(c) highlight the main product was SA. The selectivity to GBL slightly in-

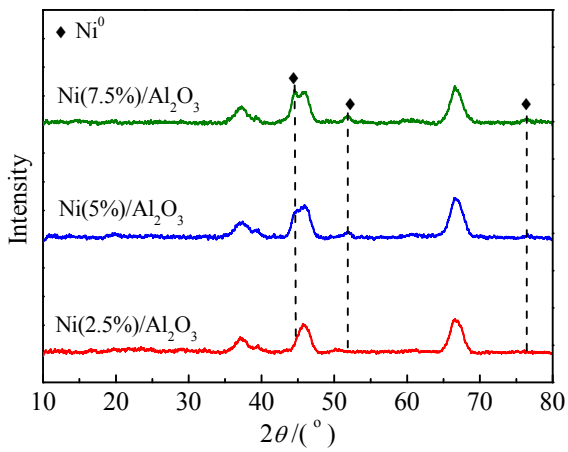

Fig. 7. XRD patterns of the catalysts reduced at 750 °C for 2 h.

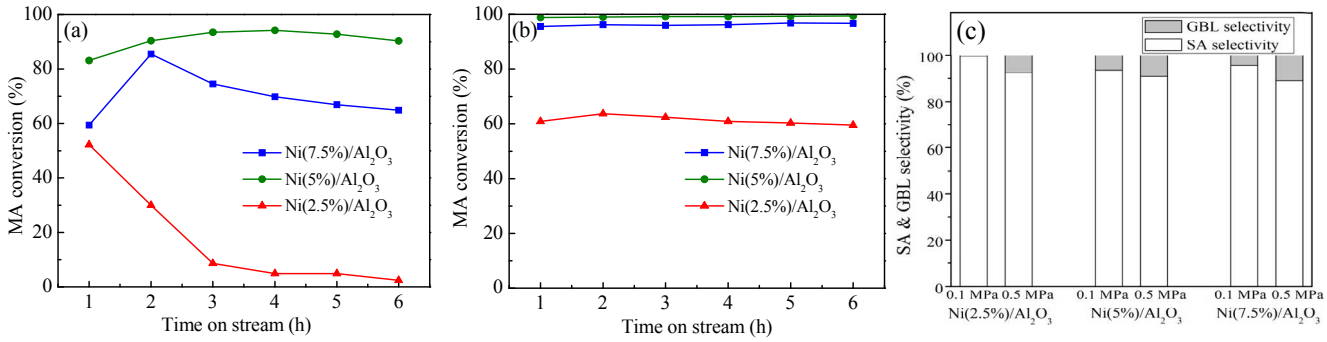

Fig. 8. MA conversion over three Ni/Al_2O_3 catalysts reduced at 750 °C for 2 h. Reaction conditions: temperature = 120 °C; WHSV (MA) = 2 h^{-1}; H_2 pressure = 0.1 MPa (a); 0.5 MPa (b); SA (black) and GBL (red) selectivities (c) (data obtained after 6 h).

creased with increasing H_2 pressure as this change promoted the hydrogenation of SA to produce GBL [10,38].

3.3. Effect of reduction temperature on catalytic activity

The reduction temperature is known to significantly influence the physicochemical properties of the catalyst, including the degree of reduction of Ni^{2+} species and the size of Ni^0 particles, and thus impact the catalytic activity [17]. The Ni(5%)/Al_2O_3 catalyst was selected as the basis for investigating the impact of the reduction temperature.

The second reaction step, the hydrolysis of SA to form GBL, produces H_2O as a by-product [39] which may react with MA to produce maleic acid. Thus, it was decided to maintain an operating temperature of over 100 °C to ensure any H_2O formed was removed from the system. Because Ni(5%)/Al_2O_3 showed high MA conversion at 120 °C with WHSV (MA) = 2 h^{-1} even under atmospheric pressure, we decided to study the catalyst reduced by H_2 at different temperatures at low MA conversion with a high WHSV (MA) = 6 h^{-1}.

The Ni(5%)/Al_2O_3 catalyst samples reduced for 2 h at 650, 700 and 750 °C were denoted as $NiAl_{650}$, $NiAl_{700}$ and $NiAl_{750}$, respectively. H_2-TPR results of calcined and reduced catalysts were the basis of analysis. The reduction degree of $NiAl_{650}$, $NiAl_{700}$ and $NiAl_{750}$ was calculated according to the corresponding H_2-TPR peak area (Table 3) using the method described in the literature [40] and found to be (13.7, 39.6 and 90.6)%, respectively. The desorption peak area of CO-TPD was used to determine the amounts of metallic Ni species and Fig. 9 shows that this increased with reduction temperature. Given that Ni species were not completely reduced, the dispersion was then corrected by the reduction degree to give (19.0, 15.2 and 8.7)% for $NiAl_{650}$, $NiAl_{700}$ and $NiAl_{750}$, respectively. The corrected dispersion results were consistent with those obtained by XRD which suggested that the Ni^0 particle size increased at higher reduction temperatures (Fig. 10).

The impact of reduction temperature on MA conversion over Ni(5%)/Al_2O_3 presented in Fig. 11 shows that the $NiAl_{700}$ catalyst exhibited the highest catalytic activity. A previous study suggested that both the amount of Ni^0 and its particle size

Table 3
Reduction degree and dispersion of the Ni(5%)/Al_2O_3 catalyst reduced at different temperature.

Reduction temperature (°C)	Reduction degree (%)	Dispersion (%)	
		Uncorrected [a]	Corrected [b]
650	13.7	2.6	19.0
700	39.6	6.0	15.2
750	90.6	7.9	8.7

[a] Uncorrected dispersion (%) = numbers of surface Ni^0 atom/(numbers of total Ni^0 atom) × 100.
[b] Corrected dispersion (%) = numbers of surface Ni^0 atom/(numbers of total Ni^0 atom × reduction degree) × 100.

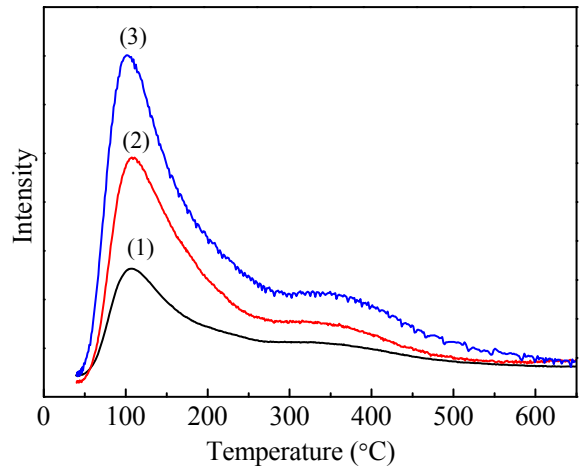

Fig. 9. CO-TPD for Ni(5%)/Al_2O_3 catalyst reduced at 650 (1), 700 (2) and 750 °C (3) for 2 h.

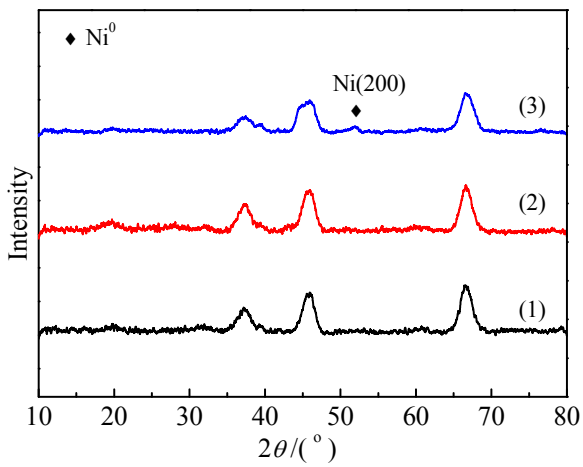

Fig. 10. XRD patterns for Ni(5%)/Al_2O_3 catalyst reduced at 650 (1), 700 (2) and 750 °C (3) for 2 h.

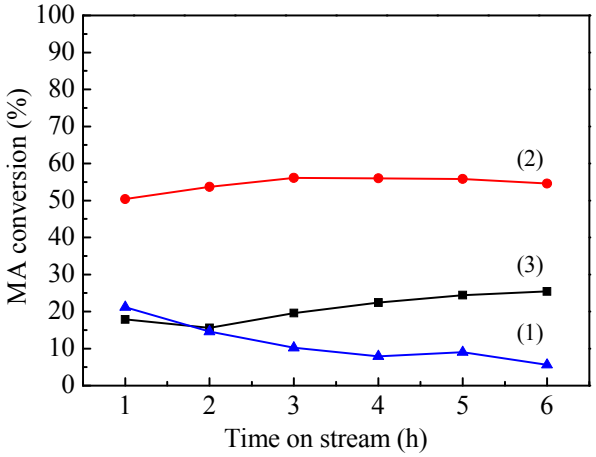

Fig. 11. MA conversion with time over Ni(5%)/Al_2O_3 reduced at 650 (1), 700 (2) and 750 °C (3) for 2 h. Reaction conditions: temperature = 120 °C, H_2 pressure = 0.5 MPa, WHSV (MA) = 6 h^{-1}.

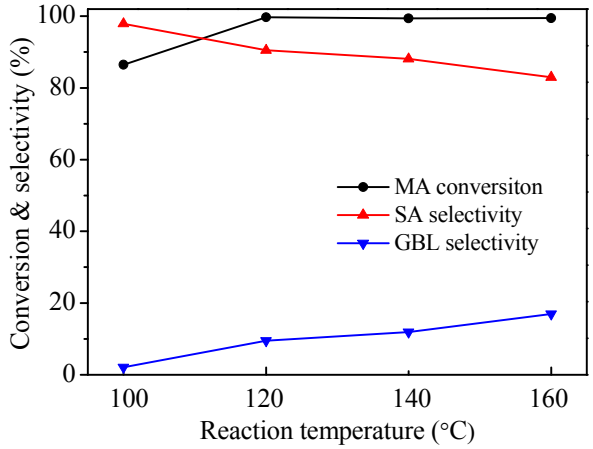

Fig. 13. Effect of reaction temperature on catalytic performance of Ni(5%)/Al_2O_3 reduced at 700 °C for 2 h. Reaction conditions: H_2 pressure = 0.5 MPa, WHSV (MA) = 2 h^{-1}. Data obtained after 6 h.

influenced the catalytic activity during the MA hydrogenation [38]. Here, the $NiAl_{650}$ catalyst exhibited the lowest catalytic activity, perhaps owing to having the least Ni^0 active sites. Conversely, although the $NiAl_{750}$ catalyst contained more Ni^0 than the $NiAl_{700}$ sample, the $NiAl_{700}$ catalyst had smaller Ni^0 particles which is thought to explain the $NiAl_{700}$ catalyst's higher catalytic activity.

The effect of WHSV on catalytic performance was investigated at 120 °C and 0.5 MPa of H_2 over Ni(5%)/Al_2O_3 reduced at 700 °C for 2 h (Fig. 12). The conversion of MA decreased with increasing WHSV and nearly 100% conversion of MA was achieved at WHSV (MA) = 1 and 2 h^{-1}. SA is an intermediate product that is produced by the hydrogenation of MA and then hydrolyzed to give GBL, the production of which is known to be favored at low WHSV values [38]. Near-100% conversion of MA with ~90% selectivity to SA was achieved at WHSV = 2 h^{-1}.

The effect of reaction temperature (100–160 °C) was investigated at 0.5 MPa of H_2 with WHSV = 2 h^{-1} over Ni(5%)/Al_2O_3 reduced at 700 °C for 2 h (Fig. 13). Both the conversion of MA and the selectivity to GBL increased with increasing temperature, which is consistent with results reported by Huo *et al.* [15], who reported a nearly 92% SA yield achieved over Ni/TiO_2 at 220 °C. This compared with a nearly 90% SA yield at 120 °C in the present work. Previous work suggested that small Ni^0 particle sizes were responsible for high catalytic activity, which may explain the present results for the spinel-derived catalysts with highly dispersed, small Ni^0 species [21].

Catalytic stability was investigated using the Ni(5%)/Al_2O_3 catalyst reduced at 700 °C for 2 h under the optimized reaction conditions of 120 °C and 0.5 MPa of H_2, which produced an SA yield of nearly 90% (Fig. 14). The chemical environment of Al atoms in the fresh and used catalysts was investigated by ^{27}Al MAS NMR experiments (Fig. 15). Resonances at δ = 63 and 6 ppm were assigned to the tetrahedral and octahedral coordinated Al species, respectively [41]. The relative population of Al species showed that the ratio of tetrahedral to octahedral Al species in the fresh and used catalysts was similar (~0.4), indicating that the support underwent no structural transformation. Consistent with these results, the XRD analysis (Fig. 16) also confirmed that the structure of the used Ni/Al_2O_3 was unchanged following the reaction.

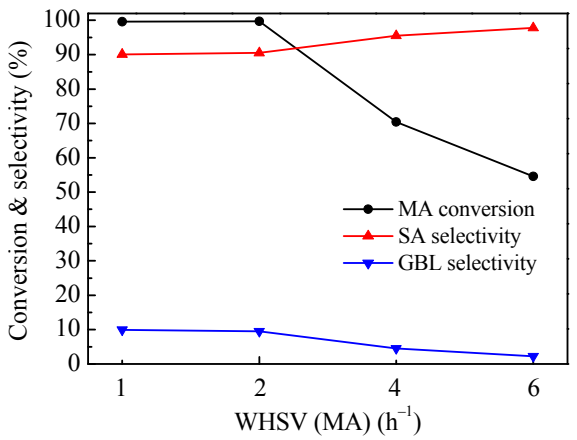

Fig. 12. Effect of WHSV on performance of Ni(5%)/Al_2O_3 reduced at 700 °C for 2 h. Reaction conditions: temperature = 120 °C, H_2 pressure = 0.5 MPa. Data obtained after 6 h.

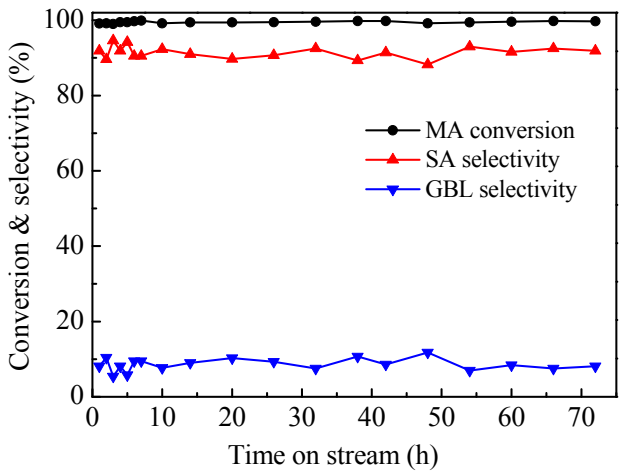

Fig. 14. Catalytic stability of Ni(5%)/Al_2O_3 at 120 °C with 0.5 MPa of H_2 and WHSV(MA) = 2 h^{-1}.

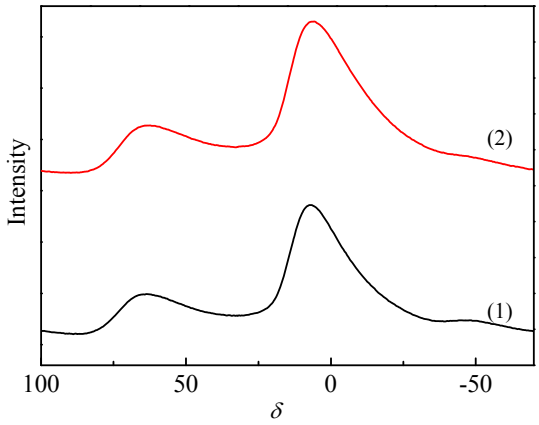

Fig. 15. ^{27}Al MAS NMR spectra of the fresh (1) and used (2) Ni(5%)/Al_2O_3.

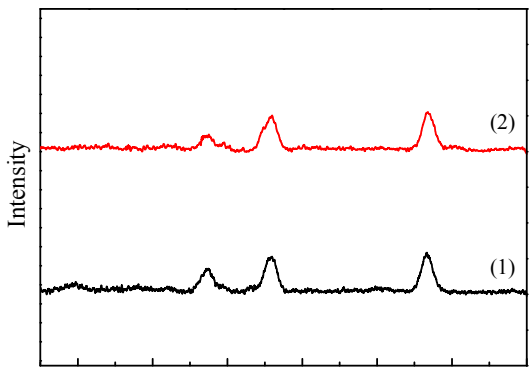

4. Conclusions

A series of Ni/Al_2O_3 spinel-derived catalysts with different levels of Ni-loading (2.5, 5 and 7.5) wt% were synthesized and studied for the low-temperature hydrogenation of MA to produce SA. Optimized preparation conditions (5% Ni-loading, reduction at 700 °C for 2 h) yielded a catalyst that possessed a large amount of well-dispersed, small Ni^0 particles yielding high catalytic activity under optimized reaction conditions (120 °C and 0.5 MPa of H_2). Long-term stability for over 72 h was achieved, with a constant near-100% conversion of MA and ~90% selectivity to SA.

References

[1] C. I. Meyer, A. J. Marchi, A. Monzon, T. F. Garetto, *Appl. Catal. A,* **2009**, 367, 122–129.
[2] R. C. Zhang, H. B. Yin, D. Z. Zhang, L. Qi, H. H. Lu, Y. T. Shen, T. S. Jiang, *Chem. Eng. J.,* **2008**, 140, 488–496.
[3] D. Z. Gao, Y. H. Feng, H. B. Yin, A. L. Wang, T. S. Jiang, *Chem. Eng. J.,* **2013**, 233, 349–359.
[4] X. Liao, Y. Zhang, M. Hill, X. Xia, Y. X. Zhao, Z. Jiang, *Appl. Catal. A,* **2014**, 488, 256–264.
[5] J. Li, L. P. Qian, L. Y. Hu, B. Yue, H. Y. He, *Chin. Chem. Lett.,* **2016**, 27, 1004–1008.
[6] H. J. Yuan, C. L. Zhang, W. T. Huo, C. L. Ning, Y. Tang, Y. Zhang, D. Q. Cong, W. X. Zhang, J. H. Luo, S. Li, Z. L. Wang, *J. Chem. Sci.,* **2014**, 126, 141–145.
[7] Y. Hara, H. Kusaka, H. Inagaki, K. Takahashi, K. Wada, *J. Catal.,* **2000**, 194, 188–197.
[8] Y. Q. Huang, Y. Ma, Y. W. Cheng, L. J. Wang, X. Li, *Appl. Catal. A,* **2015**, 495, 124–130.
[9] G. Budroni, A. Corma, *J. Catal.,* **2008**, 257, 403–408.
[10] J. Li, W. P. Tian, L. Shi, *Ind. Eng. Chem. Res.,* **2010**, 49, 11837–11840.
[11] Y. Yu, Y. L. Guo, W. C. Zhan, Y. Guo, Y. S. Wang, G. Z. Lu, *J. Mol. Catal. A,* **2014**, 392, 1–7.
[12] Y. Yu, W. C. Zhan, Y. Guo, G. Z. Lu, S. Adjimi, Y. L. Guo, *J. Mol. Catal. A,* **2014**, 395, 392–397.
[13] C. I. Meyer, S. A. Regenhardt, A. J. Marchi, T. F. Garetto, *Appl. Catal. A,* **2012**, 417–418, 59–65.
[14] S. A. Regenhardt, C. I. Meyer, T. F. Garetto, A. J. Marchi, *Appl. Catal. A,* **2012**, 449, 81–87.
[15] W. T. Huo, C. L. Zhang, H. J. Yuan, M. J. Jia, C. L. Ning, Y. Tang, Y. Zhang, J. H. Luo, Z. L. Wang, W. X. Zhang, *J. Ind. Eng. Chem.,* **2014**, 20, 4140–4145.
[16] Y. Zhang, L. L. Zhao, H. X. Zhang, H. T. Li, P. P. Liu, Y. Y. Gai, Y. X. Zhao, *CIESC.,* **2015**, 66, 2505–2513.
[17] C. I. Meyer, S. A. Regenhardt, M. E. Bertone, A. J. Marchi, T. F. Garetto, *Catal. Lett.,* **2013**, 143, 1067–1073.
[18] J. Li, W. P. Tian, X. Wang, L. Shi, *Chem. Eng. J.,* **2011**, 175, 417–422.
[19] W. P. Tian, S. F. Guo, L. Shi, Pet. *Sci. Technol.,* **2014**, 32, 1784–1790.
[20] S. F. Guo, L. Shi, *Catal. Today,* **2013**, 212, 137–141.
[21] M. E. Bertone, S. A. Regenhardt, C. I. Meyer, V. Sebastian, T. F. Garetto, A. J. Marchi, *Top. Catal.,* **2016**, 59, 159–167.
[22] P. G. Savva, K. Goundani, J. Vakros, K. Bourikas, C. Fountzoula, D. Vattis, A. Lycourghiotis, C. Kordulis, *Appl. Catal. B,* **2008**, 79, 199–207.
[23] A. L. Alberton, M. M. V. M Souza, M. Schmal, *Catal. Today,* **2007**, 123, 257–264.
[24] B. C. Lippens, J. H. de Boer, *Acta Crystal,* **1964**, 17, 1312–1321.
[25] H. T. Li, Y. L. Xu, C. G. Gao, Y. X. Zhao, *Catal. Today,* **2010**, 158,475–480.
[26] G. Paglia, C. E. Buckley, A. L. Rohl, R. D. Hart, K. Winter, A. J. Studer, B. A. Hunter, J. V. Hanna, *Chem. Mater.,* **2004**, 16, 220–236.
[27] Z. G. Hao, Q. S. Zhu, Z. Jiang, B. L. Hou, H. Z. Li, *Fuel Process. Technol.,* **2009**, 90, 113–121.
[28] G. H. Li, L. J. Hu, J. M. Hill, *Appl. Catal. A,* **2006**, 301, 16–24.
[29] Z. Ma, Q. Z. Jiang, X. Wang, W. G. Zhang, Z. F. Ma, *Catal. Commun.,* **2012**, 17, 49–53.
[30] G. Poncelet, M. A. Centeno, R. Molina, *Appl. Catal. A,* **2005**, 288, 232–242.
[31] Z. Boukha, C. Jimenez-Gonzalez, B. de Rivas, J. R. Gonzalez-Velasco, J. I. Gutierrez-Ortiz, R. Lopez-Fonseca, *Appl. Catal. B,* **2014**, 158–159, 190–201.
[32] R. Lopez-Fonseca, C. Jimenez-Gonzalez, B. de Rivas, J.I. Gutierrez-Ortiz, *Appl. Catal. A,* **2012**, 437–438, 53–62.
[33] F. Meyer, R. Hempelmann, S. Mathurband, M. Veith, *J. Mater. Chem.,* **1999**, 9, 1755–1763.
[34] C. Ragupathi, J. J. Vijaya, P. Surendhar, L. J. Kennedy, *Polyhedron,* **2014**, 72,1–7.
[35] R. Wang, Y. H. Li, R. H. Shi, M. M. Yang, *J. Mol. Catal. A,* **2011**, 344, 122–127.
[36] T. Numaguchi, H. Eida, K. Shoji, *Int. J. Hydrog. Energy,* **1997**, 22, 1111–1115.
[37] M. Tao, X. Meng, Y. H. Lu, Z. C. Bian, Z. Xin, *Fuel,* **2016**, 165, 289–297.
[38] Y. H. Feng, H. B. Yin, A. L. Wang, T. Xie, T. S. Jiang, *Appl. Catal. A,*

Graphical Abstract

Chin. J. Catal., 2017, 38: 1166–1173 doi: 10.1016/S1872-2067(17)62844-4

Ni/Al_2O_3 catalysts derived from spinel $NiAl_2O_4$ for low-temperature hydrogenation of maleic anhydride to succinic anhydride

Jie Li, Yuanhang Ren, Bin Yue *, Heyong He *
Fudan University

Ni/Al_2O_3 catalyst derived from spinel $NiAl_2O_4$ shows high performance in low-temperature hydrogenation of maleic anhydride to produce succinic anhydride. 90% yield of succinic anhydride was obtained over Ni/Al_2O_3 catalyst at 120 °C.

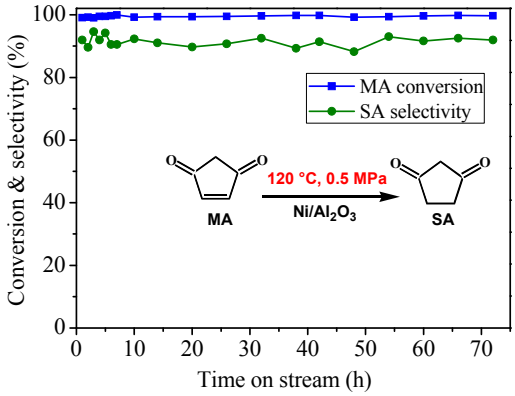

2012, 425, 205–212.
[39] J. Li, W. P. Tian, L. Shi, *Catal. Lett.*, **2011**, 141, 565–571.
[40] J. H. Song, S. J. Han, J. Yoo, S. Park, D. H. Kim, I. K. Song, *J. Mol. Catal. A*, **2016**, 415, 151–159.
[41] J. J. Fitzgerald, G. Piedra, S. F. Dec, M. Seger, G. E. Maciel, *J. Am. Chem. Soc.*, **1997**, 119, 7832–7842.

尖晶石型衍生的Ni/Al_2O_3催化剂低温催化顺酐加氢合成丁二酸酐

李 杰, 任远航, 岳 斌#, 贺鹤勇*
复旦大学化学系, 上海市分子催化与功能材料重点实验室, 上海200433

摘要: 开发高活性的顺酐加氢制丁二酸酐和γ-丁内酯催化剂具有重要的工业意义. 顺酐加氢多采用Cu基和Ni基催化剂, 但一般Cu基和Ni基催化剂存在反应温度高(170–260 °C)和稳定性差等缺点, 很有必要开发高活性的顺酐加氢催化剂. 我们以拟薄水铝石作为Al_2O_3载体的前驱体, 采用浸渍法制备了一系列镍铝尖晶石型衍生的不同Ni含量的Ni/Al_2O_3催化剂, 并研究了它们在顺酐加氢反应中的催化性能.

还原前Ni/Al_2O_3催化剂的X射线衍射结果表明, 催化剂含有$NiAl_2O_4$物种. 氮吸附结果显示, 不同Ni含量的催化剂均具有介孔结构. 氢-程序升温还原研究发现, Ni/Al_2O_3催化剂经750 °C还原2 h后, 其表面上$NiAl_2O_4$物种能被高效还原. X射线粉末衍射结果表明, 750 °C还原的Ni/Al_2O_3催化剂中金属Ni颗粒尺寸随着Ni负载量升高而增大. 利用一氧化碳-程序升温脱附对750 °C还原的Ni/Al_2O_3催化剂进行研究, 发现750 °C还原的催化剂上金属Ni物种含量从高到低依次为: Ni(7.5%)/Al_2O_3 > Ni(5%)/Al_2O_3 > Ni(2.5%)/Al_2O_3. 采用CO化学吸附获得的Ni(2.5%)/Al_2O_3, Ni(5%)/Al_2O_3和Ni(7.5%)/Al_2O_3催化剂上金属Ni颗粒尺度分别为8.0, 12.8和15.7 nm. 活性研究结果表明, 750 °C还原的Ni(5%)/Al_2O_3催化剂具有最高的催化活性, 这可能是由于Ni(5%)/Al_2O_3催化剂具有较多的Ni活性位点和较合适的Ni颗粒粒度所致. 进一步研究发现, 在650–750 °C还原温度下, Ni(5%)/Al_2O_3催化剂的还原度随着还原温度的升高而升高, Ni分散度随着还原温度的升高而降低. 活性结果研究表明, 700 °C还原的Ni(5%)/Al_2O_3催化剂具有较多的Ni活性位点和较合适的Ni颗粒粒度, 具有最高的加氢催化活性, 其在120 °C, H_2压力为0.5 MPa和质量空速为2 h^{-1}的反应条件下, 能获得近100%的顺酐转化率和90%的丁二酸酐选择性, 同时该催化剂具有优良的稳定性. 以上结果表明, 尖晶石型衍生的Ni/Al_2O_3催化剂是一个十分有应用前景的顺酐加氢催化剂.

关键词: 顺酐; 丁二酸酐; 加氢; 镍; 尖晶石

收稿日期: 2017-02-22. 接受日期: 2017-04-19. 出版日期: 2017-07-05.
*通讯联系人. 电话: (021)65643916; 传真: (021)55665572; 电子信箱: heyonghe@fudan.edu.cn
#通讯联系人. 电话: (021)65642779; 传真: (021)65338041; 电子信箱: yuebin@fudan.edu.cn
基金来源: 国家自然科学基金(21173050, 21371035); 中石化基金(X514005).
本文的英文电子版由Elsevier出版社在ScienceDirect上出版(http://www.sciencedirect.com/science/journal/18722067).